

In vitro cellular responses to silicon carbide nanoparticles: impact of physico-chemical features on pro-inflammatory and pro-oxidative effects

Jérémie Pourchez · Valérie Forest · Najih Boumahdi · Delphine Boudard · Maura Tomatis · Bice Fubini · Nathalie Herlin-Boime · Yann Leconte · Bernard Guilhot · Michèle Cottier · Philippe Grosseau

Received: 11 June 2012 / Accepted: 20 August 2012
© Springer Science+Business Media B.V. 2012

Abstract Silicon carbide is an extremely hard, wear resistant, and thermally stable material with particular photoluminescence and interesting biocompatibility properties. For this reason, it is largely employed for industrial applications such as ceramics. More recently, nano-sized SiC particles were expected to enlarge their use in several fields such as composite supports, power electronics, biomaterials, etc. However, their large-scaled development is restricted by the potential toxicity of nanoparticles related to their manipulation and inhalation. This study aimed at synthesizing (by laser pyrolysis or sol-gel methods), characterizing physico-chemical properties of six samples of SiC nanopowders, then determining their in vitro biological impact(s). Using a macrophage cell line, toxicity was assessed in terms of cell membrane

damage (LDH release), inflammatory effect (TNF- α production), and oxidative stress (reactive oxygen species generation). None of the six samples showed cytotoxicity while remarkable pro-oxidative reactions and inflammatory response were recorded, whose intensity appears related to the physico-chemical features of nano-sized SiC particles. In vitro data clearly showed an impact of the extent of nanoparticle surface area and the nature of crystalline phases (α -SiC vs. β -SiC) on the TNF- α production, a role of surface iron on free radical release, and of the oxidation state of the surface on cellular H₂O₂ production.

Keywords Silicon carbide nanoparticles · Laser pyrolysis · Sol-gel · Biological activity · Toxicity · Macrophage cell line

J. Pourchez (✉) · V. Forest
Ecole Nationale Supérieure des Mines, CIS-EMSE,
LINA EA 4624, 42023 Saint-Etienne, France
e-mail: pourchez@emse.fr

J. Pourchez · V. Forest · N. Boumahdi ·
D. Boudard · B. Guilhot · M. Cottier · P. Grosseau
SFR IFRESIS, 42023 Saint-Etienne, France

N. Boumahdi · B. Guilhot · P. Grosseau
Ecole Nationale Supérieure des Mines, SPIN-EMSE,
CNRS:FRE3312, LPMG, 42023 Saint-Etienne, France

D. Boudard · M. Cottier
Université Jean Monnet, Faculté de Médecine,
LINA EA-4624, 42023 Saint-Etienne, France

D. Boudard · M. Cottier
Université de Lyon, 42023 Saint-Etienne, France

D. Boudard · M. Cottier
CHU de Saint-Etienne, 42055 Saint-Etienne, France

M. Tomatis · B. Fubini
Dipartimento di Chimica and 'G. Scansetti'
Interdepartmental Center for Studies on Asbestos and
other Toxic Particulates, Università di Torino, Turin, Italy

N. Herlin-Boime · Y. Leconte
Laboratoire Francis Perrin, Service des Photons,
Atomes et Molécules, CEA-CNRS URA2453, IRAMIS,
CEA SACLAY, 91191 Gif sur Yvette, France

Introduction

Silicon carbide (SiC) is a well-known ceramic material with remarkable properties such as high chemical inertness, elevated thermal stability, and excellent mechanical properties. As a result, mainly as micro-sized particles, SiC is widely used for many different industrial purposes in the ceramic or composite material field. Moreover, nano-sized SiC particles are also considered as promising materials for refractory carbide nanostructured ceramics, power electronics, or catalysis supports (Melinon et al. 2007; Leconte et al. 2007). More recently, attention was paid to photoluminescence properties which strongly depend on the size of SiC nanoparticles (Fan et al. 2008; Kassiba et al. 2002). Thus, several applications using nanoscaled SiC emerged in life sciences such as the development of biomedical fluorescent probes or delivery systems of chemotherapeutic agents for cancer treatment (Duncan 2006; Botsoa et al. 2008; Tong et al. 2009). Considering all things, due to the applications proposed in diverse areas of technology, workers, consumers, and patients exposure to SiC nanoparticles should increase in the next decades.

Toxicological data available in the literature are mainly obtained from experiments conducted on micro-scaled SiC particles or fibers. It has been shown that SiC dust does not induce harmful effects on tissues, allowing to consider SiC material as quite biologically inert (Bruch et al. 1993a, b). Conversely, other studies suggest potential adverse effects induced by SiC. On one hand, in vivo exposure to SiC microparticles triggers lung inflammation (Cullen et al. 1997), granulomas (Vaughan et al. 1993), bronchoalveolar hyperplasia, and severe lung fibrotic changes (Akiyama et al. 2007). On the other hand, in vitro responses to SiC microparticles were characterized by significant cytotoxic and genotoxic effects (Vaughan et al. 1993), reactive oxygen species (ROS) generation (Svensson et al. 1997), and stimulation of pro-inflammatory cytokines production like tumor necrosis factor alpha (TNF- α) (Cullen et al. 1997). Recent in vitro studies, specifically devoted to SiC nanoparticles, highlighted an accumulation in A549 lung epithelial cells, a major cell redox status disturbance, and DNA damage (Barillet et al. 2010a, b). Thus, the authors proposed to reconsider SiC nanoparticles' biocompatibility and to handle SiC nanoparticles with caution until more toxicological information is available.

In this context, to support the growing market of SiC nanopowders and nanocomposite materials, it seems imperative to study and understand the interactions between SiC nanostructures and living cells. Consequently, we conducted a multidisciplinary study to examine the impact of physico-chemical parameters of SiC nanoparticles on in vitro cellular responses. As a matter of fact, a main challenge is the lack of comprehensive data to assess the potential toxicity of SiC nanoparticles regarding different sizes, surfaces, structures, or chemical composition. As these gaps need to be filled, we aimed at identifying physico-chemical properties of SiC nanoparticles that could affect biological activity and that could be directly related to the toxicity of the nanoparticles. In order to reach this objective, we synthesized six different SiC nanoparticles showing different sizes (from 15 to 60 nm), crystallographic structures (i.e., β -SiC corresponding to SiC-3C polytype with or without the presence of α -SiC corresponding to SiC-6H polytype), variable C/Si atomic ratio (i.e., silicon or carbon excess), surface oxidation (i.e., the formation of a silica or an oxycarbide layer around the SiC grain), or chemical surface impurities (i.e., the quantification of the amount of iron per unit surface) at the laboratory scale by the laser pyrolysis and sol-gel processes. Selectively, we also used a sample of pure α -SiC synthesized by mechanical wet-milling technique during this study. In vitro toxicological assessment was carried out using a macrophage cell line (RAW 264.7, a cultured murine macrophage widely used in nanotoxicology studies due to their phagocytosis capacity), to determine the cytotoxicity (lactate dehydrogenase (LDH) release), the pro-inflammatory response (TNF- α secretion), and the oxidative stress (H₂O₂ specific production). The potential to generate free radicals HO[•], COO^{•-} was also investigated in cell-free conditions.

Experimental

SiC nanoparticle synthesis

In this study, various SiC nanopowders were synthesized using two methods: laser pyrolysis or sol-gel process. SiC nanoparticles synthesis by continuous CO₂ laser pyrolysis has already been reported (Herlin-Boime et al. 2004). This technique is based on the interaction between a powerful laser beam and a

mixture of gaseous or liquid precursors (Leconte et al. 2007). Five SiC nanopowders (named LP1 to LP5) have been synthesized by laser pyrolysis of silane (SiH_4) and acetylene (C_2H_2) gaseous precursors (Leconte et al. 2007; Cauchetier et al. 1988). The laser radiation is absorbed by silane causing the increase of the reaction temperature. The thermal energy is then transferred to acetylene by collisions leading to molecular dissociation. This decomposition is followed by nucleation and growth of hot nanoparticles emitting an incandescent flame in the temperature range 1,200–2,000 °C. A rapid cooling at the exit of the reaction zone limits the particle size, which are collected downstream the reactor. The nanoparticles obtained by laser pyrolysis are usually of spherical shape. The control of the synthesis parameters (C/Si atomic ratio of the gaseous precursors, reactant flow rates, laser power) leads to the synthesis of SiC nanoparticles with well-defined chemical composition and degree of crystallization. Moreover, the grain size is controlled by the time of residence in the reaction zone. LP1 nanopowder corresponds to typical nanoparticles of β -SiC synthesized by laser pyrolysis. Compared to SiC LP1, SiC LP2 and LP3 samples correspond to SiC nanoparticles enriched in carbon and silicon, respectively. SiC LP4 and LP5 samples correspond to nanopowders with coarse grains of larger size voluntarily obtained during laser synthesis, respectively, by increasing particles time residence in the reactor (Cauchetier et al. 1988; Tougne et al. 1993) and with a higher laser power (Fantoni et al. 1990; Herlin-Boime et al. 2004) allowing the modification of some properties such as grain size and crystallinity.

The synthesis of SiC powder by a sol-gel process has been extensively studied for the last 20 years and used for the production of fine spherical particles of SiC (Hatakeyama and Kanzaki 1990; Seog and Kim 1993). This process is a wet-chemical technique starting from a colloidal solution (sol) which contains the precursors of an integrated network (or gel). The sol-gel process generally involves the use of metal alkoxides which undergo hydrolysis and condensation polymerization reactions to form gels. In our case, precursors are phenyl-triethoxy silane (PTES) and triethoxy silane (TEOS) which after hydrolysis and polycondensation form a colloid. After 24 h at 20 °C, the collected gel is dried (60 °C/48 h) and a thermal treatment is carried out (1,500 °C during 4 h) in argon atmosphere leading to the carbothermal reduction of SiO_2 . The nanopowder

synthesized by this chemical route (named SiC SG) corresponds to spherical nanoparticles of β -SiC.

SiC nanopowders characterization

The particles morphology is assessed by electron microscopy in the SEM mode in a field-emission scanning electron microscope (JEOL JSM-6500F). The specific surface area (SSA, m^2/g) was determined by N_2 adsorption at 77 K after out-gassing for 2 h at 200 °C (Micromeritics ASAP 2000) by means of the Brunauer-Emmet-Teller (B.E.T.) method. The density (ρ , g/cm^3) was determined using a gas pycnometer (Micromeritics AccuPyc 1330) working under helium atmosphere. Results are expressed as means of ten successive measurements on the same sample. Particle diameter (BET size, nm) was calculated as $\text{BET size} = 6,000/(\rho \times \text{SSA})$. X-ray diffraction (XRD) experiments were performed at room temperature to identify the different crystalline phases (Siemens D5000) with a semi-quantitative analysis by means of Rietveld method (Siroquant V2.5 software). The crystallite size was calculated from diffractograms using the Scherrer relation (Topaz-4P software). Concentration of constitutive elements (Si, C) and impurities (O, Fe) was deduced from elemental chemical analysis by inductively coupled plasma spectrometry (ICP, Jobin-Yvon Activa) and LECO (N/O)/(C). The oxidation of SiC nanopowders was characterized by surface analysis by photoelectron spectroscopy (XPS, Thermo VG Thetaprobe).

Free radical release

The spin trap technique (Fubini et al. 1995), with electron paramagnetic resonance (EPR), has been used to evaluate the potential of SiC nanoparticles to generate free radicals (HO^\bullet , $\text{COO}^{\bullet-}$) in aqueous suspensions. 45 mg of each powder was suspended in a buffered solution (0.5 M potassium phosphate buffer, pH 7.4) containing 0.075 M of DMPO (5-5'-dimethyl-1-pyrroline-Noxide) as spin trapping agent. The reaction was started by adding the target molecule: hydrogen peroxide (0.05 M), to mimic the contact with H_2O_2 -rich lysosomal fluids following phagocytosis of the particles by alveolar macrophages, or sodium formate (1.0 M) used as a “model” target molecule for homolytic cleavage of a carbon-hydrogen bond. The radical yield was progressively measured in

a 50 μL aliquot of the suspension up to 1 h by EPR spectroscopy (Miniscope 100 EPR spectrometer, Magnetech, Germany) using the following parameters: field center 3345 G, scan range 120 G, microwave power 10 mW, modulation amplitude 1 G, scan time 80 s, number of scans 2. The use of internal standard (Mn) enables radical activity quantification. Each experiment was repeated three times.

Cell line and culture conditions

The RAW 264.7 cell line derived from murine peritoneal macrophages (MA) transformed by the AML Virus (Abelson Murine Leukemia Virus) was provided by the ATCC Cell Biology Collection (Promochem LGC, Molsheim). Cells were cultured in Dulbecco's Modified Eagle's Medium (DMEM, Invitrogen), complemented with 10 % fetal calf serum (FCS, Invitrogen), 1 % penicillin–streptomycin (penicillin 10,000 units/mL, streptomycin 10 mg/mL; Sigma-Aldrich, Saint-Quentin Fallavier, France) and incubated at 37 °C under a 5 % carbon dioxide humidified atmosphere.

Cell viability was determined by trypan blue dye exclusion (FDA, Sigma). For each experiment, as described by Leclerc et al. (2010, 2012), cells were prepared in 96-well plates (100,000 cells/well for TNF- α and LDH assays, and 300,000 cells/well for H₂O₂ parameter) in 25 μL of complete DMEM (DMEMc). Suspensions of SiC powders were prepared in a 75 μL volume of DMEMc which were added to the culture and incubated for 90 min or 24 h at 37 °C in a 5 % CO₂ atmosphere. The granulometric stability of the suspensions was checked (dynamic light scattering, nanozetasizer, Malvern instrument) before adding to the cell suspension. Different doses were tested: 15, 30, 60, and 120 μg nanoparticles per mL of DMEMc. Negative and positive controls of toxicity, corresponding to the cells incubated alone or incubated with DQ12 quartz (Bruch et al. 2004) were included. Three independent experiments were performed for each condition.

Cytotoxicity assays

The activity of the LDH released from cells with damaged membranes in the culture supernatant was assessed after a 24 h incubation of cells with nanoparticles. The CytoTox-ONE™ homogeneous

membrane integrity assay (Promega, Charbonnières les bains, France) was used according to the manufacturer's instructions. Detection was performed using a fluorometer (Fluoroskan Ascent, Thermolabsystems), with excitation/emission wavelengths set at 530/590 nm. The activity of the released LDH was reported to that of total cellular LDH (measured after the lysis of control cells) and was expressed as a percentage of the control.

Pro-inflammatory response

Tumor necrosis factor alpha (TNF- α) production was assessed in the culture supernatant after a 24-h incubation of cells with nanoparticles. A commercial ELISA Kit (Quantikine® Mouse TNF- α Immunoassay, R&D Systems, Lille, France) was used according to the manufacturer's instructions. The optical density of each well was determined using a microplate reader (Multiskan RC, Thermolabsystems, Helsinki, Finland) set to 450 nm. A standard curve was established and results were expressed in pg/mL of TNF- α .

Oxidative stress and H₂O₂ secretion

Acute oxidative stress was assessed by the production of H₂O₂ due to cellular stress (ROS parameter) in the condition of a 90-min short-term interaction with nanoparticles. Macrophages (3.10⁵ MA/well in a 96-well plate) were incubated in their culture medium at 37 °C under a 5 % CO₂ atmosphere with the different SiC particle solutions. After this cell time contact, hydrogen peroxide H₂O₂ production was measured according to the protocol of De la Harpe and Nathan (1985). Briefly, KRPG buffer containing a mixture of scopoletin (30 μM), NaN₃ (1 mM), and horseradish peroxidase (1 unit pupurogallin/mL HPO) was added to cells. Over a 90-min period, fluorimetric determination (355/460 nm excitation/emission wavelengths) of scopoletin oxidation, catalyzed by horseradish peroxidase was measured (Fluoroskan Multiskan). Results were expressed as the quantity of H₂O₂ released by cells (nmol H₂O₂/10⁶ MA).

Statistical analysis

Results are expressed as means of three independent experiments. Statistical significance was declared when $p < 0.05$ as determined using a student test.

Results and discussion

Physico-chemical characterization of SiC nanoparticles

The six nanopowders of β -SiC (with sometimes the presence of minor α -SiC crystalline phase) were produced at the laboratory scale by sol-gel or laser pyrolysis techniques, while we selectively used a sample of pure α -SiC synthesized by mechanical wet-milling. All characterization data are summarized in Table 1. The density was quite the same for the different nanopowders ranging from 3 to 3.2 g/cm³. All batches of β -SiC and α -SiC nanoparticles exhibited spherical morphology as illustrated in Fig. 1a.

The three nanopowders—LP1, LP2, and LP3—showed very similar features in terms of size and crystallographic structure: β -SiC pure cubic phase (SiC-3C polytype), SSA from 125 to 140 m²/g, BET size from 14 to 15 nm, and crystallite size of 4 nm. The difference between the BET size and the crystallite size indicated the existence of polycrystalline nanoparticles often observed for this particle size. These 3 nanoparticles mainly differed in their C/Si atomic ratio (LP1 is stoichiometric C/Si = 1, whereas LP2 showed a carbon excess C/Si = 1.21 and LP3 a silicon excess C/Si = 0.81), inducing a difference in their surface chemical composition: LP3 nanopowder appeared more oxidized (mainly due to the excess of silicon) and contained more iron impurities than LP1 and LP2 (i.e., 7–8 % vs. 14 % of O1s, and 100–200 ppm vs. 605 ppm of iron). Let us note that the difference in chemical composition in the LP1 to LP5 samples was in good agreement with the density measurements: only the stoichiometric sample LP1 exhibited the theoretical density of SiC (i.e., 3.2). The others samples showed a slightly lower density correlated to the presence of phases with lower density (carbon or oxides). Another point concerns the presence of iron impurities in these LP samples. As the synthesis by itself occurred in a wall-free zone, the presence of iron in the nanoparticles may tentatively be attributed to interaction of highly abrasive SiC nanoparticles with metallic walls and filters of the collection zone where the particles are trapped.





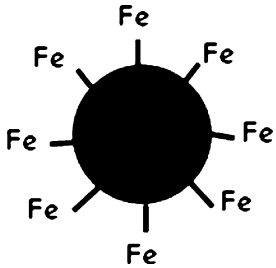
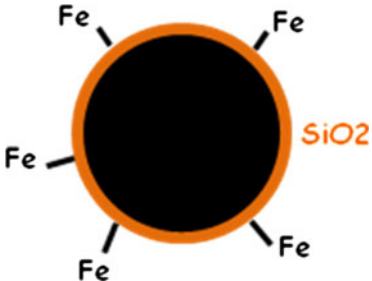

The second part of the nanoparticles range synthesized by laser pyrolysis (LP4 and LP5) was

composed of β -SiC particles having the same C/Si ratio of 0.88 (i.e., with a silicon excess) with increasing BET diameters (37 nm for LP4 vs. 59 nm for LP5), SSA (52 m²/g for LP4 vs. 33 m²/g for LP5), and crystallite size (16 nm for LP4 vs. 26 nm for LP5). In this case, the difference between the BET size and the crystallite size was too low to indicate the existence of polycrystalline nanoparticles, and was mainly due to stacking faults of cubic SiC nanograins (Fig. 1b). Moreover, the presence of α -SiC hexagonal phase (SiC-6H < 10 %) and iron impurities (around 500 ppm) was emphasized for both LP4 and LP5. The presence of SiC-6H phase was not a surprise as this crystalline phase is commonly observed in thin films (Colder et al. 2005) or gas-phase synthesized nanoparticles (Leconte et al. 2008; Tougne et al. 1993), where stacking faults can be observed within cubic SiC nanograins or crystallites. Thus, in the present case, the presence of 6H phase in XRD diagrams does not relate to a mixture of 3C nanograins with 6H grains, but to extended crystalline defects within the 3C grains (Fig. 1b, Leconte et al. 2008). Besides, LP5 exhibited a high oxidation state compared to LP4 (22 % vs. 8 % of O1s detected at the nanoparticle surface).

The batch of nanoparticles produced by the sol-gel technique showed similar crystallographic structure than LP4/LP5 (i.e., β -SiC corresponding to cubic SiC-3C polytype with the presence of α -SiC corresponding to hexagonal SiC-6H polytype lower than 10 %) and C/Si ratio (i.e., C/Si equal to 0.88), but with BET size and SSA similar to that of LP1/LP2/LP3 (i.e., BET size of 15 nm and SSA of 125 m²/g). The SG nanoparticles also showed a high purity (no iron detected) and a very low oxidation of Si atoms (8 % of O1s) at the nanoparticles surface.

Finally, we also used a sample of pure α -SiC nanoparticles (named M) to highlight the impact of the nature of the crystalline phase on the in vitro responses. The high amount of iron impurities (2,830 ppm) was in good accordance with the mechanical wet-milling technique used to synthesize this powder. As a matter of fact, LP1/LP2/LP3 are pure β -SiC (SiC-3C polytype), SG/LP4/LP5 showed the presence of α -SiC SiC-6H polytype < 10 %, and the M sample corresponded to a pure α -SiC (SiC-6H polytype).

Table 1 Physico-chemical characteristics of the six SiC nanoparticles

Sample	ρ (g/cm ³)	SSA (m ² /g)	BET size (nm)	Crystallite size	Crystalline phases	O1 s (% atomic)	Fe (ppm)	C/Si (atomic ratio)	Schematic representation
SG	3.2	125	15	14 nm monocrystalline nanograins	β -SiC (SiC-3C) α -SiC < 10 % (SiC-6H)	8	0	0.88	
LP1	3.2	139	14	4 nm polycrystalline nanograins	β -SiC (SiC-3C)	8	105	1	
LP2	3.1	125	15	4 nm polycrystalline nanograins	β -SiC (SiC-3C)	7	200	1.21	
LP3	3.0	140	14	4 nm polycrystalline nanograins	β -SiC (SiC-3C)	14 (presence of a SiO ₂ layer)	605	0.81	
LP4	3.1	52	37	16 nm nanograins with stacking faults	β -SiC (SiC-3C) α -SiC < 10 % (SiC-6H)	8	592	0.88	
LP5	3.1	33	59	26 nm nanograins with stacking faults	β -SiC (SiC-3C) α -SiC < 10 % (SiC-6H) Si (<2 %)	22 (presence of a SiO ₂ layer)	415	0.88	
M	3.0	62	32	16 nm nanograins with stacking faults	α -SiC (SiC-6H)	25 (presence of a SiO ₂ layer)	2,830	0.70	

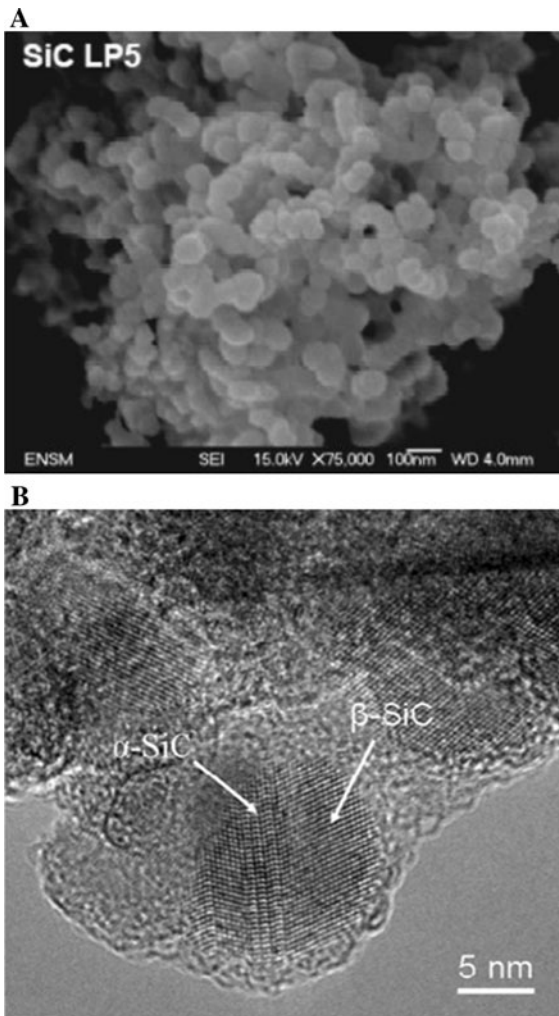


Fig. 1 Size and shape of cluster of SiC nanoparticles LP5 observed by scanning electron microscopy (a) and high-resolution transmission electron microscopy observation with the presence of α -SiC and β -SiC due to stacking faults in cubic SiC nanograins (b, Leconte et al. 2008)

In vitro cellular responses

The biological activity of SiC nanoparticles was evaluated on a macrophage cell line using four different cellular and molecular parameters: LDH release reflecting the cytotoxicity and especially the integrity of the cell membrane (Fig. 2), TNF- α production assessing the inflammatory response (Fig. 3), acute oxidative stress followed by the H₂O₂ cellular production (Fig. 4), and the capacity of nanoparticles to generate free radicals in cell-free conditions (Fig. 5).

First, no effect was observed concerning the percentage of released LDH (Fig. 2). All values in the presence of SiC nanoparticles were at the same level as the negative control (i.e., cells without nanoparticle contact), supporting the conclusion that all SiC nanoparticles studied were not cytotoxic. Only the positive control (i.e. DQ12 quartz) showed a significantly enhanced and dose-dependent LDH release.

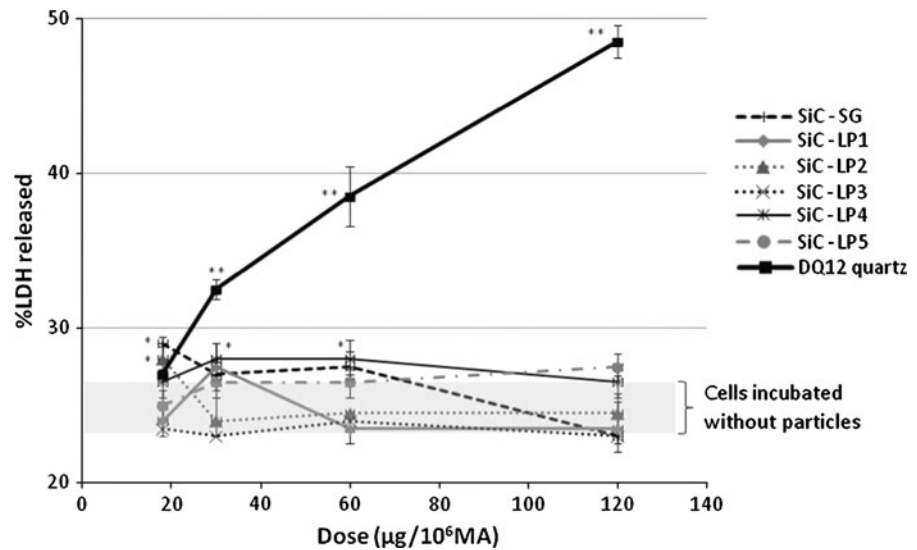
Three different behaviors were observed concerning the pro-inflammatory response induced by SiC nanoparticles. Figure 3a clearly shows that a strong variation in TNF- α concentration and a dose-response relationship occurred when the M and SG nanoparticles were incubated for 24 h with macrophages. The pro-inflammatory effect induced by the SG nanoparticles was quite similar to that of the DQ12 quartz used in this study as a positive control, while the pro-inflammatory effect induced by M was constant and significantly higher than both SG and DQ12. An intermediate pro-inflammatory response is observed for LP4 and LP5 with a significant but moderate increase of TNF- α production. Finally, LP1, LP2, and LP3 exhibited no pro-inflammatory effect as the TNF- α production remains similar to that of the negative control (i.e., cells incubated without nanoparticles).

As reported by Fig. 4, LP1, LP2, and LP3 nanoparticles induced little or no oxidative stress ($50 \text{ nmol} < \text{nH}_2\text{O}_2 < 100 \text{ nmol}$) while the H₂O₂ production was higher for LP4 and SG nanoparticles ($50 \text{ nmol} < \text{nH}_2\text{O}_2 < 180 \text{ nmol}$). The most important acute oxidative stress appeared for LP5 ($150 \text{ nmol} < \text{nH}_2\text{O}_2 < 250 \text{ nmol}$). Finally, in cell-free conditions, no radical release was observed for LP1 and SG. LP2 and LP3 were able to generate COO^{•-}, but not HO[•] radicals. Significant HO[•] radical release was observed for LP4 ($\text{nsHO}^{\bullet} = 21 \text{ nmol/m}^2$) and more importantly for LP5 (Fig. 5). This sample exhibited the highest activity in COO^{•-} ($\text{ns COO}^{\bullet-} = 400 \text{ nmol/m}^2$) and HO[•] generation per unit surface (47 nmol/m^2). LP5 also contained the highest amount of surface iron (about $11 \text{ }\mu\text{g/m}^2$).

Impact of C/Si atomic ratio on the in vitro cellular responses

LP1, LP2, and LP3 were three SiC nanoparticles showing similar crystallite size (4 nm), BET size (14–15 nm), SSA (125–139 m²/g), and oxidation state

Fig. 2 Cytotoxicity of SiC nanoparticles determined by the LDH release (reported to that of total cellular LDH measured after control cells lysis). Standard deviation and statistically significant differences from the negative control (cells incubated without nanoparticles) are also indicated: * $p < 0.05$, ** $p < 0.01$



of the surface (7–8 % of O1s) but increasing C/Si atomic ratio from 0.88 to 1.21 (Table 1). This nanoparticle panel does not differ by their cytotoxicity (no cell membrane impairment detected, Fig. 2) and their pro-inflammatory response (TNF- α values at the same level as the negative control, Fig. 3a). Thus, no influence of the C/Si atomic ratio on the in vitro cellular responses was highlighted.

Impact of SiC nanoparticle crystallite size and crystalline phase on the in vitro cellular responses

On the one hand, SG and LP1, LP2, LP3 were nanoparticles with identical BET size (14–15 nm) and disparate crystallite size (14 for SG vs. 4 nm for LP1/LP2/LP3). Indeed, SG was the only SiC nanoparticles for which BET and crystallite size were identical; whereas for the other nanoparticles, the crystallite size was lower than the BET size. As a result, SG was the only mono-crystallite SiC nanoparticle. Besides, a strong difference on the TNF- α production was observed between SG on one hand and LP1, LP2, and LP3 on the other hand (Fig. 3a). As a matter of fact, the SG monocrystallite nanoparticles triggered a TNF- α production similar to that of quartz DQ12, while SG showed a silicon oxycarbide layer (and not a silica layer) at its surface.

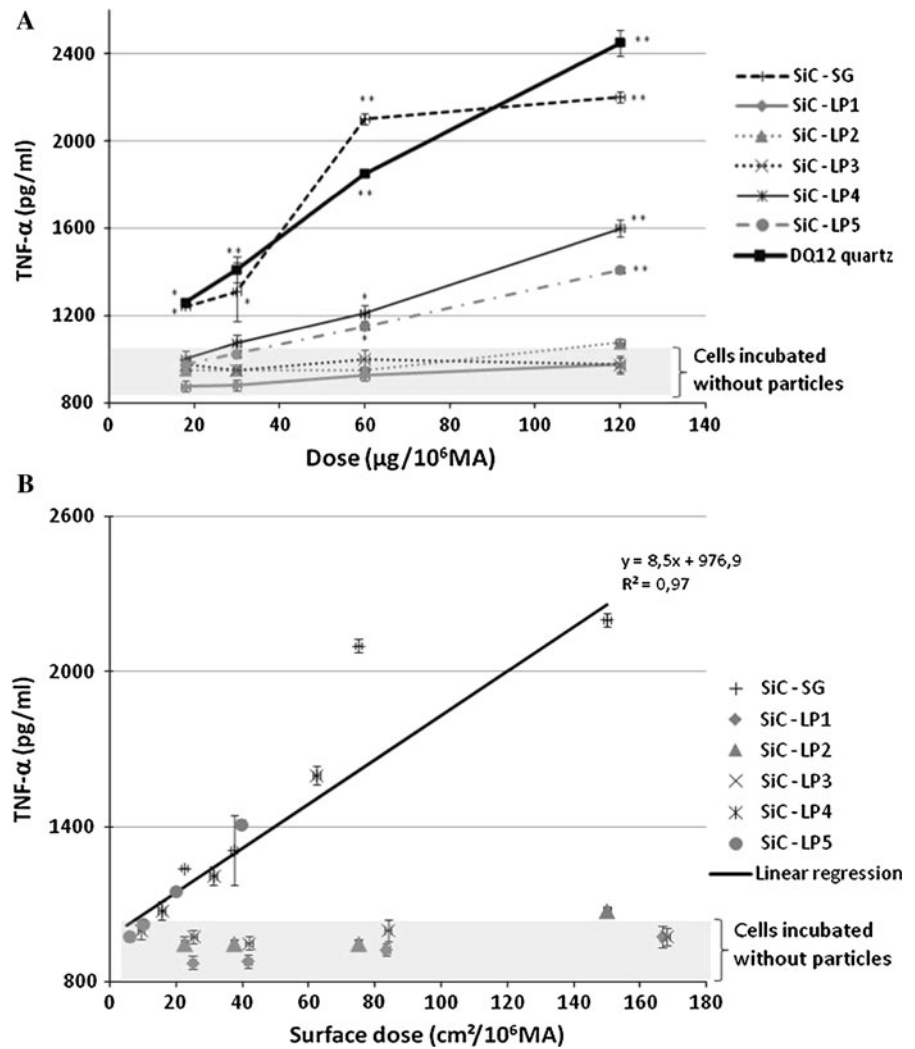
On the other hand, the impact of the presence α -SiC on the pro-inflammatory response was clearly put in evidence. Based on the range of SiC nanoparticles

synthesized at the laboratory scale, when the presence of α -SiC was detected by XRD analysis a moderate or elevated TNF- α production was observed (i.e., SG/LP4/LP5, Fig. 3a) while no pro-inflammatory response was highlighted where the nanoparticles were composed of pure β -SiC crystalline phase (i.e., LP1/LP2/LP3, Fig. 3a). The use of the sample M confirmed that the α -SiC crystalline phase induces a higher TNF- α production by comparison of β -SiC nanoparticles (data not shown, constant level of TNF- α production at $2,000 \pm 220$ pg/mL whatever the dose in the range 20–120 $\mu\text{g}/10^6$ MA). Therefore, it strongly suggests that the crystallite size and the presence of β -SiC (i.e., SiC-6H hexagonal polytype) play a major role on the pro-inflammatory response.

Impact of nanoparticle specific surface area on the in vitro cellular responses

Focusing on SG, LP4, and LP5, an influence of SiC nanoparticle surface area was observed on the pro-inflammatory effect. If we express the dose of nanoparticles in surface instead of in mass (Fig. 3b), a correlation between the TNF- α production and the SiC nanoparticles introduced in wells can be highlighted. Indeed, including 10 different points coming from SiC showing a significant TNF- α production (i.e., SG, LP5 and LP4), a linear correlation was observed ($R^2 = 0.97$). This correlation was obtained for β -SiC nanoparticles with the presence of α -SiC lower than 10 % (i.e., SG, LP5 and LP4), confirming

Fig. 3 Pro-inflammatory effect determined by the TNF- α production after a 24-h incubation of cells with SiC nanoparticles. Doses were expressed in mass (a) or surface (b). Results are means of three independent experiments. Standard deviation and statistically significant differences from the negative control (cells incubated without nanoparticles) are also indicated: * $p < 0.05$, ** $p < 0.01$



the impact of both the crystalline phase and the SSA. Considering all things, the specific surface area appears as a key parameter on the pro-inflammatory response when nanoparticles containing α -SiC crystalline phase are incubated with macrophages.

Impact of the iron content on nanoparticles surface on the in vitro cellular responses

An important influence of the iron impurities was highlighted on the capacity of nanoparticles to generate free radicals both in cellular test (Akhtar et al. 2010; Kagan et al. 2006) and in cell-free condition (Turci et al. 2010; Ball et al. 2002). Ferrous ions (Fe^{2+}) may generate hydroxyl radicals through the Fenton reaction ($\text{Fe}^{2+} + \text{H}_2\text{O}_2 \rightarrow \text{Fe}^{3+} + \text{OH}^- + \text{HO}^\bullet$)

(Prousek 2007). Metallic iron (Fe^0) and ferric ions (Fe^{3+}) can produce HO^\bullet radicals through a Fenton-like mechanism where Fe^{2+} is generated by oxidation of Fe^0 (Keenan et al. 2009) by O_2 or H_2O_2 , mainly at acidic pH, and reduction of Fe^{3+} by endogenous reductants such as ascorbic acid or superoxide anion. In this context, it is not surprising to highlight a correlation between the iron content at the SiC nanoparticles surface and the production of hydroxyl radicals.

Impact of the surface oxidation of SiC nanoparticles on the in vitro cellular responses

The XPS analysis clearly demonstrated that all SiC nanoparticles exhibit a more or less important surface oxidation (Table 1). However, results showed that

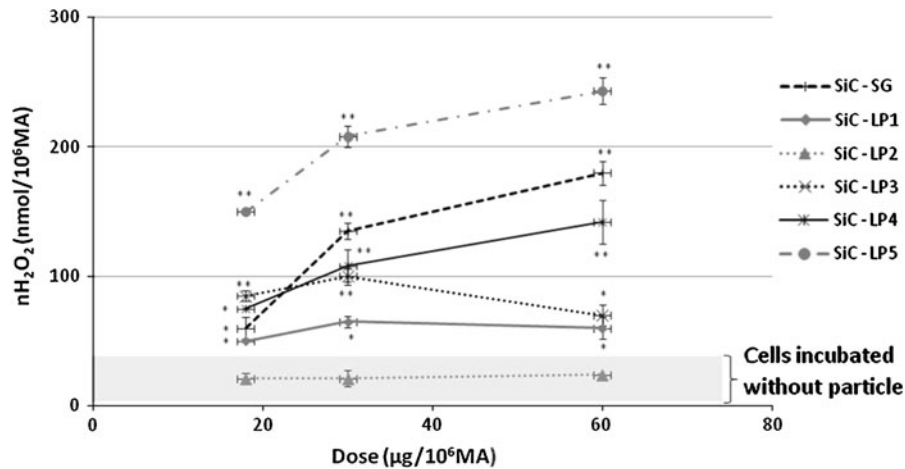


Fig. 4 Acute oxidative stress induced by the different SiC nanoparticles as assessed by the H₂O₂ production. Results are means of three independent experiments. Standard deviation

and statistically significant differences from the negative control (cells incubated without nanoparticles) are also indicated: **p* < 0.05, ***p* < 0.01

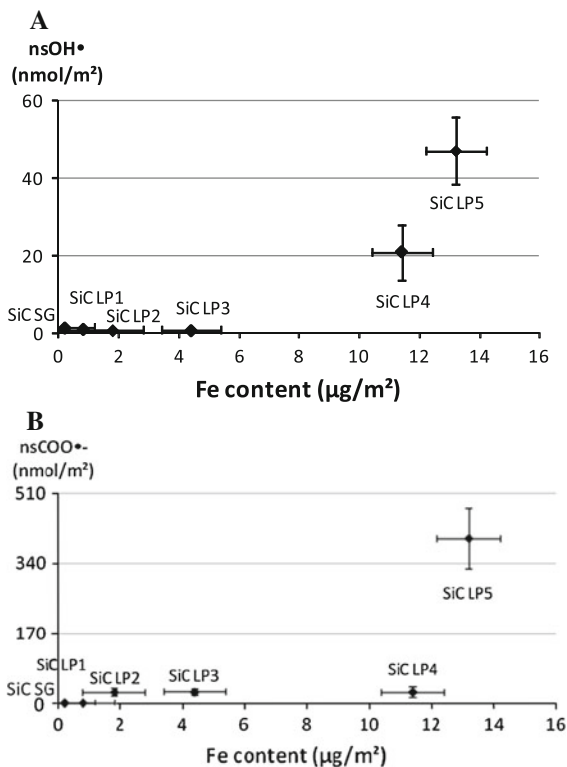


Fig. 5 Influence of iron impurities contained in the different SiC nanoparticles on the free radical release **a** HO• and **b** COO•⁻, as determined by electron paramagnetic resonance

LP5 and LP3 seem to be more oxidized with a formation of a silica phase layer (Si–O₂) whereas SG, LP1, LP2, and LP4 rather exhibit the formation of a

thin layer of silicon oxycarbide phases (Si–O_x–C_y). If we compare the biological activity of LP5 and LP4, quite similar in their physico-chemical features except the presence of a silica layer for LP5, no specific difference appears concerning the TNF-α production. Thus the nature of the surface oxidation layer (silica vs. silicon oxycarbide) does not seem to have a significant influence on the pro-inflammatory response. Moreover, even if LP5 and LP3 with a silica phase layer induce a significant H₂O₂ production, other SiC nanoparticles having a thin layer of silicon oxycarbide phases (such as LP4) exhibit similar or higher H₂O₂ production. As a result, different kinds of surface oxidation layer of SiC nanoparticle could partially mediate the H₂O₂ cellular production.

Conclusion

The toxicity of nanoparticles is known to be closely related to their physico-chemical characteristics (size, shape, surface area, chemical composition, etc.). In order to deepen such a relationship, an accurate physico-chemical characterization of different SiC nanopowders associated with an in vitro global evaluation of their biological activity were carried out. Results clearly showed the impact of C/Si atomic ratio, specific surface area, crystallite size, crystallite phase, surface oxidation, and iron impurities on cellular response (Table 2). Interestingly, opposite to

Table 2 Summary of the physico-chemical features influencing the biological activity of SiC nanoparticles

In vitro cellular responses	Physico-chemical features of the SiC nanoparticles				
	Stoichiometry (C/Si ratio)	Surface area	Crystallinity (phase, crystallite size)	Surface oxidation	[Fe] at the surface
Cytotoxicity (LDH)			No cytotoxic effect observed		
Pro-inflammatory effect (TNF- α)		Linear correlation	Correlation		
Oxidative stress					
Cellular H ₂ O ₂ production				Correlation	
HO [•] release in cell-free condition					Correlation with a threshold effect

what happens with other toxic particles, e.g., silica (Fubini et al. 2001), we show here that all the types of SiC nanoparticles tested did not induce any cytotoxic effect. By contrast, cellular responses of variable intensity—related to oxidative stress and inflammation—were observed, depending on the physico-chemical features of the nano-sized SiC particles. First, a linear correlation was observed between the surface area of SiC nanoparticles and TNF- α production. The crystallite size and the presence of the α -SiC crystalline phase also seemed to have a strong impact on the pro-inflammatory response. Moreover, the different kinds of surface oxidation layer of SiC nanoparticles (the presence of silica vs. silicon oxycarbide layer) seemed to partially mediate the H₂O₂ cellular production. Finally, the free radical production in acellular conditions seems to be associated with the iron content at the nanoparticles surface. However, opposite to other cases (e.g., silica, asbestos) in which even traces of iron ions are able to trigger the Fenton reaction (Fubini et al. 2001; Turci et al. 2010), for SiC nanoparticles a threshold effect around 11 $\mu\text{g}/\text{m}^2$ has been observed.

Few studies were devoted to the toxicity of SiC nanoparticles. The data presented in this paper support the conclusion that the commonly accepted SiC biocompatibility should be reconsidered for nano-sized particles in agreement with recent studies (Barillet et al. 2010a, b). SiC nanoparticles cannot be considered as totally biologically inert materials. Even if SiC nanoparticles do not exert any cytotoxic effects, the limited—though sometimes significant—pro-inflammatory response and/or oxidative stress suggest

a potential toxicity in cellular cultures that should be further investigated.

Further investigations are also necessary to a better understanding of the relationship between SiC physico-chemical features, cellular responses, and the underlying mechanisms. However, this multidisciplinary study can be helpful in the frame of the design approach to achieve safer SiC-based nanotechnology (Morose 2010). Indeed, it appears more cautious for companies to try to mitigate the potential risks of nanoparticles during the design stage rather than downstream during manufacturing or customer use. This is why, using safer design principles, at least four parameters (i.e., surface area, crystallite size, nature of crystallite phase, and iron content) should be well-controlled not only to preserve the desired product functionality but also to reduce at the same time the potential hazard of SiC nanoparticles, particularly as far as pro-inflammatory responses and the free radicals release are concerned.

References

- Akhtar MJ, Kumar S, Murthy RC et al (2010) The primary role of iron-mediated lipid peroxidation in the differential cytotoxicity caused by two varieties of talc nanoparticles on A549 cells and lipid peroxidation inhibitory effect exerted by ascorbic acid. *Toxicol In Vitro* 24(4): 1139–1147
- Akiyama I, Ogami A, Oyabu T et al (2007) Pulmonary effects and biopersistence of deposited silicon carbide whisker after 1-year inhalation in rats. *Inhalation Toxicol* 19(2): 141–147

- Ball BR, Smith KR, Veranth JM et al (2002) Bioavailability of iron from coal fly ash: mechanisms of mobilization and of biological effects. *Inhalation Toxicol* 12(4):209–225
- Barillet S, Jugan M, Laye M et al (2010a) In vitro evaluation of SiC nanoparticles impact on A549 pulmonary cells: cyto-, genotoxicity and oxidative stress. *Toxicol Lett* 198(3): 324–330
- Barillet S, Simon-Deckers A, Herlin-Boime N et al (2010b) Toxicological consequences of TiO₂, SiC nanoparticles and multi-walled carbon nanotubes exposure in several mammalian cell types: an in vitro study. *J Nanopart Res* 12(1):61–73
- Botsoa J, Lysenko V, Geloan A et al (2008) Application of 3C-SiC quantum dots for living cell imaging. *Appl Phys Lett* 92(17):173902–173903
- Bruch J, Rehn B, Song H et al (1993a) Toxicological investigations on silicon-carbide. 1 inhalation studies. *Br J Ind Med* 50(9):797–806
- Bruch J, Rehn B, Song H et al (1993b) Toxicological investigations on silicon-carbide. 2 in vitro cell tests and long-term injection tests. *Br J Ind Med* 50(9):807–813
- Bruch J, Rehn S, Rehn B et al (2004) Variation of biological responses to different respirable quartz flours determined by a vector model. *Int J Hyg Environ Heal* 207:203–216
- Cauchetier M, Croix O, Luce M (1988) Laser synthesis of silicon carbide powders from silane and hydroxycarbon mixtures. *Adv Ceram Mater* 3:548–552
- Colder H, Rizk R, Morales M et al (2005) Influence of substrate temperature on growth of nanocrystalline silicon. *J Appl Phys* 98:024313
- Cullen RT, Miller BG, Davis JMG et al (1997) Short-term inhalation and in vitro tests as predictors of fiber pathogenicity. *Environ Health Perspect* 105(5):1235–1240
- De la Harpe J, Nathan CF (1985) A semi-automated micro-assay for H₂O₂ release by human-blood monocytes and mouse peritoneal-macrophages. *J Immunol Methods* 78(2): 323–336
- Duncan R (2006) Polymer conjugates as anticancer nanomedicines. *Nat Rev Cancer* 6(9):688–701
- Fan J, Li H, Jiang J et al (2008) 3C-SiC nanocrystals as fluorescent biological labels. *Small* 4:1058–1062
- Fantoni R, Borsella E, Piccirillo S et al (1990) Laser synthesis and crystallographic characterization of ultrafine SiC powders. *J Mater Res* 5(1):143–150
- Fubini B, Mollo L, Giamello E (1995) Free radical generation at the solid/liquid interface in iron containing minerals. *Free Rad Res* 23:593–614
- Fubini B, Fenoglio I, Elias Z et al (2001) Variability of biological responses to silicas: effect of origin, crystallinity, and state of surface on generation of reactive oxygen species and morphological transformation of mammalian cells. *J Environ Pathol Toxicol Oncol* 20(1):95–108
- Hatakeyama F, Kanzaki S (1990) Synthesis of monodispersed β -spherical SiC powder by a sol-gel process. *J Am Ceram Soc* 73(7):2107–2110
- Herlin-Boime N, Vicens J, Dufour C et al (2004) Flame temperature effect on the structure of SiC nanoparticles grown by laser pyrolysis. *J Nanopart Res* 6(1):63–70
- Kagan VE, Tyurina YY, Tyurin VA et al (2006) Direct and indirect effects of single walled carbon nanotubes on RAW 264.7 macrophages: role of iron. *Toxicol Lett* 165(1): 88–100
- Kassiba A, Makowska-Janusik M, Bouclé J et al (2002) Photoluminescence features on the Raman spectra of quasi-stoichiometric SiC nanoparticles: experimental and numerical simulations. *Phys Rev B* 66:155317
- Keenan CR, Goth-Goldstein R, Lucas D et al (2009) Oxidative stress induced by zero-valent iron nanoparticles and Fe(II) in human bronchial epithelial cells. *Environ Sci Technol* 43(12):4555–4560
- Leclerc L, Boudard D, Pourchez J et al (2010) Quantification of microsized fluorescent particles phagocytosis to a better knowledge of toxicity mechanisms. *Inhal Toxicol* 22:1091–1100
- Leclerc L, Rima W, Boudard D et al (2012) Size of submicrometric and nanometric particles affect cellular uptake and biological activity of macrophages in vitro. *Inhal Toxicol* 24(9):580–588
- Leconte Y, Maskrot H, Combemale L et al (2007) Application of the laser pyrolysis to the synthesis of SiC, TiC and ZrC pre-ceramics nanopowders. *J Anal Appl Pyrol* 79:465–470
- Leconte Y, Leparoux M, Portier X, Herlin-Boime N et al (2008) Controlled synthesis of β -SiC nanopowders with variable stoichiometry using inductively coupled plasma. *Plasma Chem Plasma Process* 28:233
- Melinon P, Masenelli B, Tournus F et al (2007) Playing with carbon and silicon at the nanoscale. *Nat Mater* 6(7): 479–490
- Morose G (2010) The 5 principles of “design for safer nanotechnology”. *J Clean Prod* 18:285–289
- Prousek J (2007) Fenton chemistry in biology and medicine. *Pure Appl Chem* 79(12):2325–2338
- Seog IS, Kim CH (1993) Preparation of monodispersed spherical silicon carbide by the sol-gel method. *J Mater Sci* 28:3277
- Svensson I, Arturson E, Leanderson P et al (1997) Toxicity in vitro of some silicon carbides and silicon nitrides: whiskers and powders. *Am J Ind Med* 31:335–343
- Tong R, Christian DA, Tang L et al (2009) Nanopolymeric therapeutics. *MRS Bull* 34(6):422–431
- Toungne P, Hommel H, Legrand AP et al (1993) Evolution of the structure of ultrafine SiC-laser formed powders with synthesis conditions. *Diamond Relat Mater* 2:486
- Turci F, Tomatis M, Lesci IG et al (2010) The iron-related molecular toxicity mechanism of synthetic asbestos nanofibres: a model study for high-aspect-ratio nanoparticles. *Chemistry* 17(1):350–358
- Vaughan GL, Trently SA, Wilson RB (1993) Pulmonary response, in vivo, to silicon-carbide whiskers. *Environ Res* 63(2):191–201